



1 Drought disrupts atmospheric carbon uptake in a 2 Mediterranean saline lake

3 Ihab Alfadhel^{1,2}, Ignacio Peralta-Maraver^{1,2,3*}, Isabel Reche^{1,3}, Enrique P.
4 Sánchez-Cañete^{2,4,5}, Sergio Aranda-Barranco^{1,4}, Eva Rodríguez-Velasco^{1,3},
5 Andrew S. Kowalski^{2,4,5}, Penélope Serrano-Ortiz^{1,4*}.

6 7 *Authors adress:*

8 ¹Departamento de Ecología, Facultad de Ciencias, Universidad de Granada, Granada,
9 Spain.

10 ²Instituto del Agua, Granada, Universidad de Granada, Spain.

11 ³Research Unit Modeling Nature (MNat), Universidad de Granada, Granada, Spain.

12 ⁴Instituto Interuniversitario de Investigación del Sistema Tierra en Andalucía (IISTA),
13 Universidad de Granada, Spain

14 ⁵Departamento de Física Aplicada, Universidad de Granada, Granada, Spain.

15

16 **Correspondence to:* Ignacio Peralta-Maraver (peraltamaraver@ugr.es) and Penélope
17 Serrano-Ortiz (penelope@go.ugr.es).

18

19 **Abstract:** Saline inland lakes play a key role in the global carbon cycle, acting as
20 dynamic zones for atmospheric carbon exchange and storage. Given the global decline of
21 saline lakes and the expected increase of periods of drought in a climate change scenario,
22 changes in their potential capacity to uptake or emit atmospheric carbon are expected.
23 Here, we conducted continuous measurements of CO₂ and CH₄ fluxes at the ecosystem
24 scale in a saline endorheic lake of the Mediterranean region over nearly 2 years. Our focus
25 was on determining net CO₂ and CH₄ exchanges with the atmosphere under both dry and
26 flooded conditions, using the eddy covariance (EC) method. We coupled greenhouse gas
27 flux measurements with water storage and analyzed meteorological variables like air
28 temperature and radiation, known to influence carbon fluxes in lakes. This extensive data
29 integration enabled the projection of the net carbon flux over time, accounting for both
30 dry and wet periods on an interannual scale. We found that the system acts as a significant
31 carbon sink by atmospheric CO₂ uptake in wet conditions, with uptake ceasing in periods
32 of drought. Moreover, increased air temperatures during wet phases slightly decrease the



33 CO₂ uptake efficiency. Regarding CH₄, we measured uptake rates that exceeded those of
34 well-aerated soils such as forest soils or grasslands. Additionally, we observed that CH₄
35 uptake during dry periods was nearly double that of wet periods. However, the absence
36 of continuous data prevented us from correlating CH₄ uptake processes with potential
37 environmental predictors. Our study challenges the widespread notion that wetlands are
38 universally greenhouse gas emitters, highlighting the significant role that endorheic saline
39 lakes can play as natural sink of atmospheric carbon. However, our work also underscores
40 the vulnerability of these ecosystem services in the current climate change scenario,
41 where drought episodes are expected to become more frequent and intense in the coming
42 years.

43

44 **Keywords:** Intermittent saline lake, eddy covariance, greenhouse gas fluxes, ecosystem
45 metabolism, Mediterranean shallow lake

46

47 1. Introduction

48 Saline inland lakes are diverse and play a crucial role in the global carbon cycle, serving
49 as dynamic zones for carbon dioxide exchange with the atmosphere (Li et al. 2022; Liao
50 et al. 2024) and long-term sinks of organic and inorganic carbon (Anderson and Stedmon
51 2007; Song et al. 2013; Li et al. 2017). In limnology, however, the ecological importance
52 of these systems has only recently been recognized, despite they account for
53 approximately 44% of global lake volume and 23% of lake surface area (Messenger et al.,
54 2016). Saline lakes vary in size from ephemeral ponds to extensive deep-water bodies,
55 such as the Caspian Sea (Eugster and Hardie, 1978). These lakes are characterized by
56 salinity levels that exceed 3 parts per thousand and are notably isolated from a direct
57 marine influence (Williams, 2002; Wang et al., 2018). They are found in endorheic
58 (hydrologically landlocked) basins across a wide array of climates, spanning cold to
59 warm/hot arid regions in all continents, including Antarctica (Williams, 2002; Wang et
60 al., 2018). As terminal points in many hydrological networks, they collect not only
61 significant amounts of salts but also nutrients and organic and inorganic carbon
62 (Anderson and Stedmon 2007; Song et al. 2013; Batanero et al. 2017; Li et al. 2017; Liao
63 et al. 2024).

64 The first estimations about the role of saline lakes on global carbon fluxes
65 suggested that these lakes might function as hotspots for the CO₂ emission (Duarte et al.,



66 2008). However, more recent works point out that saline lakes have lower partial pressure
67 of CO₂ (pCO₂) than freshwater lakes (Wan et al. 2017) and some systems appear to
68 uptake CO₂ during the winter (Li et al., 2022) or annually (Yang et al. 2021). Therefore,
69 more seasonal studies on CO₂ fluxes in saline lakes are need it to understand the
70 conditions when these systems behave as sink or sources of CO₂. Variations in CO₂ and
71 CH₄ flux estimates across different studies of water bodies are primarily due to the highly
72 variable data obtained from discrete sampling (Li et al. 2022) or because of differences
73 in sampling seasons at the intra-annual scale (Liao et al. 2024). Meanwhile, gathering
74 continuous time series data on CO₂ and CH₄ sequestration and emission fluxes over years
75 is needed for accurate assessment of the net carbon balance in inland water systems
76 (Martínez-García et al. 2024). Nevertheless, long-term, uninterrupted, and direct
77 monitoring of greenhouse gas flux dynamics at the ecosystem level is relatively scarce in
78 aquatic ecosystems, and this is particularly true for saline lakes. To the best of our
79 knowledge, only a couple of studies have reported continuous year-round direct
80 measurements at the ecosystem scale for CO₂ fluxes (Yang et al. 2021; Li et al. 2022).
81 However, saline lakes' characteristics differ with latitude (Hammer 1986) and could have
82 very different behaviors regarding carbon exchanges depending on climate conditions.

83 The carbon hydrochemistry in permanent saline lakes, especially in mountainous
84 and Arctic latitudes such as the Tibetan Plateau or Svalbard is largely influenced by
85 surface ice formation (Anderson et al., 2004; Rysgaard et al., 2012, 2013; Wu et al., 2014;
86 Yan and Zheng, 2015). In contrast, saline lakes in arid and semi-arid endorheic basins,
87 including Mediterranean climates, are typically shallow, often ephemeral, and/or
88 hypersaline due to evaporation exceeding precipitation (García et al., 1997; Batanero et
89 al. 2017; Saccò et al., 2021). The lower depths and higher surface-to-volume ratio, driven
90 by drought conditions, induce significant physicochemical fluctuations in these saline
91 inland water bodies, spanning from diurnal to interannual scales (Comin et al. 1990;
92 García and Niell 1991; García et al. 1997; Batanero et al. 2017). Consequently, the
93 precipitation regime and subsequent changes in groundwater levels determine the ecology
94 of saline lakes in arid and semi-arid regions. However, research on the interannual
95 variability of carbon fluxes in saline lakes affected by seasonal flooding and drought is
96 lacking. This knowledge gap urgently requires focused research to elucidate the impacts
97 of climatic variability on the carbon dynamics of these ecosystems, which have been
98 identified as particularly vulnerable to climate fluctuations (Tweed et al., 2011).
99 Furthermore, recent studies highlight a global decline in lake water storage in most



100 endorheic basins and in the Sahara, Arabia, Southern Europe basin in particular (Wang et
101 al. 2018), a situation expected to worsen with more severe droughts in a climate change
102 scenario, leading to lower water levels and prolonged desiccation periods (Wurtsbaugh et
103 al., 2017; Hassani et al., 2020).

104 In this study, we carried out continuous and interannual measurements of CO₂ and
105 CH₄ fluxes at the ecosystem level in the saline lake Fuente de Piedra using the Eddy
106 Covariance (EC) method. Serving as a model of a Mediterranean shallow saline lake, it
107 is characterized by sporadic episodes of water retention but predominantly dry during the
108 summer. The objectives of our work are a) to quantify carbon exchanges during the dry
109 and the flooded conditions, determining its role as a carbon source or sink, b) to evaluate
110 main drivers promoting carbon exchange behaviors, and finally c) to model the annual
111 net carbon flux of the system as a function of its meteorological drivers. Our research
112 aims to enhance our understanding of the carbon dynamics and the impacts of climate
113 change on the net carbon balance in Mediterranean intermittent endorheic lakes.

114

115 **2. Material and methods**

116 *Study Site*

117 Fuente de Piedra is a shallow and saline lake located in an endorheic basin in the province
118 of Málaga, Andalusia, Spain (37.11 N, -4.77 W, elevation 410 m: **Fig 1**). It spans
119 approximately 17 km², measuring 6.8 km in length and 2.5 km in width, with a maximum
120 depth of 1.5 meters. We take advantage of Fuente de Piedra Lake's inclusion in the
121 Ramsar Convention in 1983. This designation ensures a rich history monitoring of water
122 storage and the meteorological drivers discussed in this article. Such a comprehensive
123 dataset allows for the back projection of the net carbon flux of the system over time,
124 incorporating both dry and wet periods at an interannual scale. This lake is recognized as
125 a vital habitat within a protected wetland at various levels—regional (as a natural reserve),
126 European (designated as a special bird protection area), and international (acknowledged
127 as a Ramsar site)—and offers an exemplary nesting ground for the pink flamingo
128 (*Phoenicopterus roseus*), largely due to its shallow waters. Among primary producers,
129 diatoms constitute the largest fraction of primary producers of the phytoplankton
130 through the year, being dominated by *Hantzschia amphioxys*, *Amphora coffeiformis*,
131 *Stauronensis amphioxys*, *Cocconeis placentula*, *Entomoneis* sp. and several species of
132 *Navicula* and *Nitzschia* sp. (García and Niell, 1993).



133 Salinity levels in the lake vary significantly, ranging from oligosaline (5 ppt) to
134 hypersaline conditions (> 200 ppt), influenced by the annual hydrological cycle (Batanero
135 et al. 2017). This cycle is delineated into two distinct phases: a pooling phase during
136 autumn and winter (December to March), and an evaporative and drought phase spanning
137 spring and summer (April to November). The lake primarily receives water from
138 groundwater inflow (Rodríguez- Rodríguez et al. 2006), complemented by contributions
139 from two streams (**Fig. 1**) and surface runoff from surrounding farmlands. Notably, the
140 stream entering from the northeast adds nutrients. However, sediment samples distributed
141 across the lake and analyzed through combustion (Heiri et al., 2001) showed it to be
142 homogeneous in organic carbon (0.21 ± 0.069 mg C), nitrogen (0.015 ± 0.004 mg N) and
143 the C:N ratio (14.4 ± 2.26).

144

145 *Field measurements of greenhouse gas fluxes and meteorological drivers.*

146 We employed the eddy covariance method to quantify the exchanges of CO₂, CH₄, and
147 energy (sensible and latent heat) every 30 min from August 2021 to May 2023. Thus,
148 eddy covariance system was operated for more than 21 months, including two dry periods
149 in summer. An open-path eddy covariance (EC) system was strategically positioned atop
150 a tower, 3.1 meters above ground level, on the western bank of the lake (**Fig.1**). This setup
151 included two open-path infrared gas analyzers: the LI7500 for CO₂ and water vapor, and
152 the LI7700 for CH₄ (LICOR Inc., Lincoln, NE, USA). Wind vector components (u, v, w)
153 and sonic temperature were accurately measured using a sonic anemometer (R.M. Young
154 81000V, Traverse City, MI, USA). Both instruments recorded the data at a frequency of
155 10Hz.

156 In addition to gas measurements, we measured a comprehensive suite of
157 environmental and soil state variables every 10 seconds to capture the conditions over a
158 representative ground surface area and collected every 30 min average by a data logger
159 (CR1000, Campbell Scientific, Logan, UT, USA). A quantum sensor (LI190, Lincoln,
160 NE, USA) was utilized to measure the vertical component of the incoming photosynthetic
161 photon flux density (PPFD) at a height of 2.9 meters. Air temperature (T_a) and relative
162 humidity (RH) were monitored using a thermohygrometer (HMP 45C, Campbell
163 Scientific, Logan, UT, USA). Net radiation (R_n) was quantified by a net radiometer (NR
164 Lite, Kipp and Zonen, Delft, Netherlands). Soil heat flow (G) calculations were facilitated
165 by one heat flux plate (HFP01SC, Hukseflux, Delft, Netherlands) placed at 8 cm depth,
166 complemented by three pairs of soil temperature probes (TCAV, Campbell Scientific,



167 Logan, UT, USA) situated at depths of 4 cm and lateral distances of 3.20 m, 6.34 m, and
168 8.90 m from the tower.

169 The groundwater level (GWL) was monitored daily using a piezometer situated
170 within a well in the salt flats, approximately 2 kilometres south of the EC tower and on
171 the opposite side of the lake (37.1071° N, -4.7631° W). Furthermore, data on daily
172 precipitation (PPT), air temperature, and incident solar radiation (spanning wavelengths
173 from 350 to 1100 nm) were acquired from a meteorological station located adjacent to
174 Fuente de Piedra Lake, in Sierra Yeguas (37.1383° N, -4.8358°; 467 m.a.s.l.). The tower
175 setup and instruments were maintained (mainly cleaning lenses of the open path sensors)
176 every two weeks.

177

178 ***Greenhouse gas flux data processing, quality control and partitioning***

179 Half-hourly means (48 measurements per day), variances, and covariances of greenhouse
180 gas fluxes, adhering to the principles of Reynolds decomposition, were calculated using
181 the EddyPro® 7.0.7 software (Li-Cor), according to international standards and protocols
182 (Sabbatini et al., 2018). The data processing protocol encompassed the following steps:
183 (1) axis rotation for tilt correction using the double rotation method (Wilczak et al., 2001),
184 (2) turbulent fluctuations were calculated using block averaging method, (3) time lag was
185 compensated by covariance maximization with default, (4) Webb–Pearman–Leuning
186 (WPL) correction of air density fluctuation (Webb et al., 1980), (5) despiking and raw
187 data statistical screening (Vickers and Mahrt, 1997) and (6) spectral corrections of high-
188 and low-pass filtering effects. Regarding the latter, high-frequency loss due to path
189 averaging, signal attenuation and sensor separation was compensated according to
190 Moncrieff et al., (1997), whereas low-frequency loss due to finite time averaging length
191 and detrending was corrected according to Moncrieff et al., (2004). Quality check flags
192 were calculated for flux data according to the widely adopted methodology combining
193 two tests: steady state test and the developed turbulent conditions test. Over the study
194 period, we only selected high-quality fluxes (flag value =0) measured when the open-path
195 sensors were totally clean according to their respective AGC values (AGC value equal to
196 56 for Open path LI-7500A CO₂ /H₂O analyzer and AGC value equal to or higher than
197 20 for LI-7700.

198 To quantify the sampling area of flux measurements, a footprint model was
199 estimated using the method by Kljun et al., (2004) (**Fig 1**). Data periods when the wind
200 comes from terrestrial adjacent environment (251° to 59°) were rejected, representing



201 between 45% and 70% of the available daytime and night-time data respectively during
202 the dry season (GWL=0), and 30% of the available daytime and night-time data
203 respectively during the wet seasons (GWL>0). Overall, for the nearly 2 years of
204 measurements, 18% and 8% of the potential daytime data were of good quality for CO₂
205 and CH₄ fluxes respectively. Whereas for night-time the available data were reduced to
206 10 and 5% respectively. The energy balance closure (ratio of the sum of sensible and
207 latent turbulent fluxes, H + LE, to the net radiation minus soil heat flux, R_n - G) was 76%
208 (R² = 0.64; n = 3117).

209

210 *Predicting greenhouse gas fluxes as responses to meteorological drivers*

211 We examine the relationship of CO₂ and CH₄ fluxes in response to groundwater level,
212 serving as a proxy for long-term water storage, with air temperature as the main factor
213 regulating respiration in the system, and incident solar radiation modulating the
214 photosynthetic rate. Since these variables were measured every 24-hour, we processed
215 half-hourly CO₂ and CH₄ fluxes collected to construct 24-hour integrated values. We
216 selected dates that contained over 50% of the anticipated data points, particularly those
217 with more than 25 valid measurements distributed during the day, to calculate integrated
218 daily flux. Selecting 26 and Y days for CO₂ and CH₄, respectively, well distributed
219 throughout the measured period (both dry and wet periods). Before integrating daily flux
220 values, we filled gaps in the half-hourly CO₂ and CH₄ flux data using linear interpolation
221 for missing values. This selection criterion aimed to accurately represent the daily pattern
222 in flux measurement distribution.

223 To analyze the relationship between integrated daily fluxes and their potential
224 environmental predictors, we employed a linear regression combined with a forward
225 model selection technique (Aho et al 2014). This method involved sequentially fitting a
226 series of regression models, each incorporating different combinations of predictors and
227 their interactions. The process began with simple models, each containing only one
228 primary predictor, and gradually increased in complexity to include all possible
229 interactions among predictors. We then used the Akaike Information Criterion (AIC) to
230 evaluate and identify the most effective model from the set. The model with the lowest
231 AIC was selected as the best fit, indicating it provides the most useful balance between
232 model complexity and explanatory power. After selecting the model, we examined the
233 influence of the predictors by analyzing the slope β coefficients at a significance level of



234 $\alpha = 0.05$, using a 95% confidence interval to determine if these coefficients were
235 significantly different from zero.

236 Additionally, while ground water level (GWL) was measured daily, our model
237 selection process also aimed to identify which daily measurements of air temperature and
238 incident solar radiation (mean, minimum, or maximum) were the best predictors. This
239 method ensured that the chosen model was robust and relevant to the ecological scales
240 being studied. Detailed instructions on how to run these analyses are detailed in the R
241 script available in DRYAD (see details in the *data accessibility statement* section).

242

243 3. Results

244 *Time series of greenhouse gas emissions and meteorological drivers*

245 At Fuente de Piedra Lake, we observed significant seasonal variations in meteorological
246 conditions, as illustrated in **Fig 2A**. Air temperature (T_a) and incident solar radiation
247 exhibited consistent trends throughout the study period, with mean daily values of 17 ± 7
248 $^{\circ}\text{C}$ for T_a and $18 \pm 8 \text{ MJ m}^{-2} \text{ d}^{-1}$ for incident solar radiation. In contrast, these two
249 environmental variables generally followed asynchronous patterns with groundwater
250 level (GWL) and precipitation events (**Fig 2A and B**). Particularly during the summer
251 months (July, August, September), the highest daily air temperature values coincided with
252 GWLs beneath the surface and a lack of precipitation. Also, during the "dry" periods, a
253 salt crust several centimeters thick developed on the sediment (see Figure 3B). For
254 instance, the minimum T_a recorded was 2°C in January 2023 corresponding with a period
255 of frequent precipitation and GWL above the surface. Conversely, the maximum T_a of 34
256 $^{\circ}\text{C}$ occurred in August 2021, during a period when the GWL was 24 cm below the surface.

257 We observed a strong correspondence between water storage in Fuente de Piedra
258 Lake and its capacity to assimilate atmospheric CO_2 . The CO_2 flux patterns can be
259 categorized into two distinct lake states: a flooded lake (groundwater level >0 cm,
260 indicated from purple to blue colour in **Fig 2C and D**) and a dry lake (groundwater level
261 <0 cm, shown from orange to yellow colour). During periods of flooding, the lake acted
262 as a CO_2 sink, with fluxes ranging from 0 to $-30 \mu\text{mol m}^{-2} \text{ s}^{-1}$. The CO_2 assimilation
263 capacity increases with groundwater level and incident solar radiation, particularly from
264 January to June. Notably, the flooded periods in the two years of the study showed marked
265 differences in groundwater level. In 2022, we recorded the highest CO_2 uptake of $30 \mu\text{mol}$
266 $\text{m}^{-2} \text{ s}^{-1}$ in May, when the groundwater level was at its peak, 40 cm above the surface. The



267 peak CO₂ uptake in 2023 was approximately half of what was observed in 2022. Although
268 this peak occurred in March rather than May, it followed a similar trend to the ground
269 water level (GWL), which was also about half of the peak level observed in 2022 (~20
270 cm above the surface). In contrast, under dry conditions, Fuente de Piedra Lake ceases
271 the CO₂ uptake, occasionally transitioning to minor CO₂ emissions. Notice that during
272 extreme rainfall pulses within dry periods, when Fuente de Piedra Lake remained
273 relatively dry with the groundwater level below the surface, we observed notable net CO₂
274 emissions. For example, a heavy rainfall event in September 2021 (36 mm day⁻¹) resulted
275 in CO₂ emissions reaching up to 10 μmol m⁻² s⁻¹, with a high elevation of the groundwater
276 level above the surface (from -20 to near 20 cm). Also, in October of both 2021 and 2022,
277 subsequent rainfall events (12 mm day⁻¹ and 22 mm day⁻¹, respectively) corresponded
278 with CO₂ emissions of 7 μmol m⁻² s⁻¹ and 5.5 μmol m⁻² s⁻¹, respectively. In these cases,
279 emissions occurred under negative GWL conditions.

280

281 In the case of CH₄, flux was relatively stable throughout the whole study period,
282 generally acting as a sink, with values fluctuating between -0.2 and 0.1 μmol m⁻² s⁻¹ (**Fig**
283 **2D**). Furthermore, no clear relationship was observed between CH₄ fluxes, and the
284 meteorological variables examined.

285

286 *Fluxes of CO₂ and CH₄ at a daily scale*

287 When examining the daily scale during wet periods, it becomes evident that CO₂
288 assimilation predominantly takes place during daylight hours, specifically between 9 am
289 and 2 pm (local time) (**Fig. 3**). It should be noted that the few emission values observed
290 within this time frame correspond to the emission occurrences described earlier for the
291 dry season, which promptly followed rainfall events. In the case of the dry period, it is
292 noteworthy that a salt crust forms over the lake, leading to a near cessation of CO₂ fluxes.
293 In the case of CH₄, there is also a discernible increase in assimilation fluxes between 9
294 am and 2 pm. This observed pattern is consistent in both wet and dry conditions.

295

296 *Model predictions of 24-hour integrated flux values in the study system*

297 A clear pattern in CH₄ flux was not detected during the study period. Likewise, no clear
298 relationship with the environmental predictors studied could be identified. Additionally,
299 measurements obtained from the EC tower resulted in a substantial number of gaps in the
300 CH₄ time series, making it impossible to establish a predictive model for these fluxes. On



301 the contrary, we were able to adjust a robust regression model for CO₂ integrated daily
302 flux. A total of 26 daily integrated CO₂ flux values were obtained for the sampling period,
303 analyzing those dates when more than 25 valid measurements were available. After AIC
304 model selection routine, the candidate predictive model for daily integrated CO₂ flux was
305 determined to include groundwater level, maximum daily air temperature, and mean
306 incident solar radiation. Additionally, the model incorporated interactions between
307 groundwater level and maximum daily air temperature, as well as between groundwater
308 level and incident solar radiation (Summary Table of the model is available in the
309 Supplementary Material). Indeed, fitted statistical capacity of the model has a relatively
310 high explanatory capability (Adjusted R²=0.72).

311 The model confirmed a positive effect of groundwater level on enhancing CO₂
312 assimilation in the system (**Fig 4A**; $\beta_{GWL} = -0.115$, 95% CI = -0.214 to -0.016; note that
313 assimilation corresponds with negative values of the CO₂ flux). While the isolated impact
314 of air temperature increase on CO₂ assimilation could not be determined ($\beta_{Ta} = +0.07$,
315 95%CI = -0.053 to +0.192), the model identified an antagonistic interaction between air
316 temperature and groundwater level ($\beta_{GWL \times Ta} = +0.010$, 95%CI = +0.005 to +0.015). As
317 air temperature increases, the positive effect of GWL on CO₂ assimilation diminishes (**Fig**
318 **4B**). Conversely, mean daily incident solar radiation was found to promote CO₂
319 assimilation ($\beta_{Rad} = -0.12$, 95%CI = -0.21 to -0.03), with a pronounced synergy between
320 mean daily incident solar radiation and the presence of water ($\beta_{GWL \times Rad} = 95\%CI = -$
321 0.0116 to -0.003), notably enhancing the capacity for CO₂ assimilation (**Fig 4C**).

322 Using time series data for groundwater level, daily maximum air temperature, and
323 mean daily incident solar radiation at Fuente de Piedra Lake, we generated retrospective
324 predictions of CO₂ assimilation capacity in the system dating back to 2001 (**Fig 4D**). The
325 model predictions closely aligned with the observed values for the study period when
326 using the time series data for the predictors, supporting the robust predictive ability of our
327 model (Supplementary Material; **Fig S1**). Our estimates indicate a pronounced fluctuation
328 in CO₂ assimilation capacity according to hydrological variations. In years with higher
329 groundwater level and prolonged water storage the model predicted an exceptionally high
330 capacity for atmospheric CO₂ assimilation of the lake, with annual values surpassing 0.7
331 Kg C m² year⁻¹ (e.g., in 2011, 2012, 2014, 2020). In contrast, during years marked by
332 extended droughts, a substantial reduction in CO₂ assimilation capacity was modeled.
333 These drought periods, characterized by dry conditions, resulted in a reduction of the



334 assimilation capacity to less than a third of the levels recorded in wet years (e.g., from
335 2006 to 2010).

336

337 **4. Discussion**

338 In agreement with previous research in permanent saline lakes of the Tibetan plateau (Li
339 et al. 2022), we show that a model Mediterranean shallow saline lake acts as a significant
340 carbon sink through the uptake of atmospheric CO₂ when flooded. Conversely, CO₂
341 assimilation ceases during dry periods. Longitudinal time series analysis reveals that
342 prolonged droughts indeed hinder the ability of the system to assimilate atmospheric CO₂
343 due to the lack of water, but we also observed that an increase in air temperature during
344 wet periods moderates the CO₂ net assimilation capacity, a process likely related to the
345 reduction of gas water solubility with temperature. This underscores the pronounced
346 impact of seasonal and interannual variability, ultimately dictated by drought and rainfall
347 patterns, on the ability of the studied system to sequester atmospheric carbon. Moreover,
348 this pattern also displayed considerable variability at the daily scale, closely correlating
349 with fluctuations in incident solar radiation over daily cycles. In this regard, the CO₂
350 assimilation capacity of the system peaked during those hours of maximum incident solar
351 radiation. While measurement of CO₂ (and CH₄) fluxes at multiple scales is challenging
352 and requires specialized equipment (i.e. eddy covariance sensors), our research proposes
353 an alternative proxy. By integrating data from environmental predictors at various scales,
354 we have achieved highly accurate predictions of CO₂ exchanges between Fuente de
355 Piedra Lake and the atmosphere. In essence, we estimate CO₂ flux through the continuous
356 measuring of accessible environmental variables, namely, the amount of water, air
357 temperature, and incident solar radiation.

358 In shallow, well-mixed, and oxygenated systems like Fuente de Piedra Lake, the
359 photosynthetic capacity of the phytoplankton community is closely linked to the water
360 column height (i.e. groundwater level) (Batanero et al. 2017), promoting CO₂ assimilation
361 as the extent of the habitat for these communities expands (Wetzel, 2001). Related to the
362 aforementioned, a significant synergy exists between water storage in the ecosystem and
363 incident radiation, serving as a proxy for the photosynthetically active radiation upon
364 which photosynthesis depends. This interaction occurs on both a daily scale, associated
365 with variations in light intensity following day-night cycles, and an annual seasonal scale,
366 largely determined by changes in daylight hours throughout the year. Notably, during the



367 night, the net exchange of CO₂ between the water and the atmosphere in Fuente de Piedra
368 Lake is negligible. This could be attributed to the absence of photosynthesis during
369 nighttime. Additionally, the high salinity inherent to these environments constrains
370 methanogenesis, which is the least energy-efficient carbon mineralization process in the
371 redox sequence (reviewed in Soued et al., 2024). Considering the above, it appears to
372 offer a plausible explanation for why microbial respiration does not surpass inorganic
373 carbon assimilation through photosynthesis in systems like Fuente de Piedra Lake during
374 wet periods, despite the high content of dissolved organic carbon (Batanero et al., 2017).

375 What is more, despite the lack of CH₄ flux data, our results position Fuente de
376 Piedra lake as a CH₄ sink. Vast approximation estimates determined that Fuente de Piedra
377 could uptake on average 1.83 mg C m⁻² day⁻¹ and 3.70 mg C m⁻² day⁻¹ during the wet and
378 the dry period respectively (Supplementary Material; **Fig S2**). Such values are even higher
379 than those measured in typical well aerated soils such as soil forest or grasslands, with
380 average rates of 0.4-1.26 mg C m⁻² day⁻¹ (Murguia-Flores et al., 2021; Perez-Quezada et
381 al., 2021). The double value of uptake during the dry periods compared to the wet ones
382 appear to be consistent with some proposed mechanisms promoting CH₄
383 reduction according to the existing literature, since the increase of temperature together
384 with gas diffusivity due to loss of water, may increase methane oxydation in a similar
385 way to terrestrial ecosystems (Chen et al., 2010; Rafalska et al 2023). However, caution
386 is needed when interpreting our results, as the dynamics of methane fluxes could become
387 very complex in an intermittent system like Fuente de Piedra. On the one hand, just as
388 methanogenic activity is inhibited by salinity (Herbert et al., 2015), methanotrophic
389 activity has also been observed to be significantly reduced by salinity in terrestrial
390 systems (Ho et al., 2018). However, methane oxydation processes associated with aquatic
391 prokaryotes may be more resistant to salinity (Khmelenina et al., 2010; Deng et al. 2017),
392 especially if the variation is gradual (Osudar et al., 2017). Thus, further measurements
393 and analysis are needed to estimate the role of methane oxydation and the relevance of
394 saline intermitent lakes as CH₄ sinks in a climate change scenario.

395 Drought periods are accompanied by an increase in air temperature, with the high
396 air temperatures recorded immediately before the system completely dries out. We have
397 found that this rise in air temperature leads to a reduction of the system's capacity to
398 assimilate CO₂, even during wet conditions. A direct consequence of climatic warming is
399 the reduction of gas solubility accentuated in saline wetlands (Batanero et al. 2022) . In
400 addition, increase in temperature can enhance microbial metabolic rates and therefore,



401 biomass-specific CO₂ production (Smith et al. 2019). Given that endorheic saline lakes
402 are fueled by significant amounts of organic matter (Li et al., 2017; Batanero et al., 2017;
403 Song et al., 2013), it is unsurprising that warming leads to a decrease in net primary
404 production in the system as a result of enhanced microbial respiration, and consequently,
405 a reduction in CO₂ assimilation capacity. In addition, carbon emissions in inland waters
406 could increase with warming, independently of organic carbon inputs, simply because the
407 apparent activation energy is predicted to be higher for respiration than photosynthesis
408 (Yvon-Durocher et al. 2010; Yvon-Durocher et al. 2012). Finally, it has been recognized
409 that photosynthesis is often the first process to be affected by environmental stressors,
410 with photosynthetic capacity diminishing prior to other cellular functions (Feller, 2016;
411 Cardona et al., 2018). Specifically, carbon assimilation through the Calvin–Benson cycle
412 exhibits particular vulnerability to both drought and elevated temperatures, occurring
413 even when photosynthetic electron transport continues to operate effectively (Sharkey,
414 2005). On the whole, we show the profound synergy between global warming and
415 intensifying drought severity and frequency, disrupting the CO₂ assimilation capacity of
416 Mediterranean saline lakes and leading to negative feedback loops.

417

418 **5. Conclusion**

419 While the desiccation of saline lakes is not novel, with researchers highlighting
420 the concerning increase in dry periods within many of these ecosystems over recent
421 decades (Williams 1993; Gross 2017; Wurtsbaugh et al. 2017; Wang et al. 2018), our
422 study underscores the significant implications this has for the ecosystem services they
423 support. Our retrospective predictions show that in wet years, the system could exhibit a
424 high CO₂ assimilation rate. For instance, between 2010 and 2015, we estimated that
425 Fuente de Piedra Lake had an average assimilation rate of 0.83 (SD = ±0.27) kg C m⁻²
426 year⁻¹, comparable to the net assimilation observed in evergreen or deciduous forest
427 systems (Pastorello et al., 2020). This result challenges the generalised belief that inland
428 waters primarily act as sources of greenhouse gases (Raymond et al. 2013). Conversely,
429 the system undergoes significant reductions in its annual atmospheric CO₂ sequestration
430 capacity during dry periods. For instance, under severe drought conditions as observed in
431 Fuente de Piedra from 2005 to 2009, the annual CO₂ sequestration is estimated to have
432 fallen to less than a quarter of what was observed in more humid periods. Climate change
433 projections, including even the most optimistic scenarios, forecast an increase in both the



434 frequency and duration of heatwaves and droughts in the coming years (Trenberth 2011,
435 Perkins-Kirkpatrick 2020). This implies that saline lake ecosystems in arid and semi-arid
436 endorheic basins will remain dry for longer periods, or may even vanish, resulting in the
437 loss of a significant carbon sequestration pathway. Importantly, the disappearance of
438 saline lakes due to water scarcity has been largely attributed to anthropogenic water
439 overuse (i.e., agriculture) rather than to macroclimatic phenomena (Wurtsbaugh et al.
440 2017). This seems to be the case of Fuente de Piedra Lake, as the catchment area is
441 dominated by agricultural land. Thus, a proper water management during drought periods
442 seems to be the most plausible solution to preserve the ecosystem services provided by
443 Mediterranean saline lakes.

444

445

446 **Author contribution**

447 PS-O and IR conceived the study; all authors contributed to the installation and
448 maintenance of the eddy covariance tower; IA led the fieldwork and the processing of the
449 samples with the help of the rest of the authors; IP-M carried out the analyses and the
450 preparation of the results; IA, IP-M, and PS-O conducted the preparation of the first draft
451 of the work; all authors participated in the drafting of the final draft.

452

453 **Data accessibility statement**

454 The R script used to conduct the data analysis and the datasets are available at the Dryad
455 Digital Repository:

456 <https://datadryad.org/stash/share/qEpPRJopVR132UszL3bnaxoZh07ADL0E5LpVL6xC>

457 [SZA](#)

458

459

460 **Financial support**

461 This work was partially support by the projects PID2020-117825GB-C21 and PID2020-
462 117825GB-C22 funded by MCIN/AEI/10.13039/501100011033, LifeWatch-2019-10-
463 UGR-01 and LifeWatch-2019-09-CSIC-13 funded by the MCIN through the FEDER
464 funds from the Spanish Pluriregional Operational Program 2014-2020 (POPE),
465 LifeWatch-ERIC action line and project BAGAMET (P20_00016) funded by the
466 Counseling of Economy, Innovation, Science and Employment from the Government of
467 Andalucía, including European Union ERDF funds. I.P.-M. developed his research as



468 part of the eWARM project, supported by the Marie Skłodowska-Curie postdoctoral
469 fellowship 2022 (project number 101110111).

470

471 **Competing interests**

472 The authors declare that they have no conflict of interest.

473

474

475 **References**

476 Aho, K., Derryberry, D., and Peterson, T: Model selection for ecologists: the worldviews
477 of AIC and BIC. *Ecology*, 95(3), 631-636, <https://doi.org/10.1890/13-1452.1> ,
478 2014.

479 Anderson, L. G., Falck, E., Jones, E. P., Jutterström, S., and Swift, J. H: Enhanced uptake
480 of atmospheric CO₂ during freezing of seawater: A field study in Storfjorden,
481 Svalbard. *J. Geophys. Res. Oceans*, 109(C6)
482 <https://doi.org/10.1029/2003JC002120>, 2024.

483 Anderson, N. J., and Stedmon, C. A: The effect of evapoconcentration on dissolved
484 organic carbon concentration and quality in lakes of SW Greenland. *Freshwater
485 Biology*, 52(2), 280-289, <https://doi.org/10.1111/j.1365-2427.2006.01688.x> ,
486 2007.

487 Batanero, G. L., León-Palmero, E., Li, L., Green, A. J., Rendón-Martos, M., Suttle, C.
488 A., and Reche, I. Flamingos and drought as drivers of nutrients and microbial
489 dynamics in a saline lake. *Scientific Reports*, 7(1), 12173,
490 <https://doi.org/10.1038/s41598-017-12462-9> , 2017.

491 Batanero, G. L., Green, A. J., Amat, J. A., Vittecoq, M., Suttle, C. A., and Reche, I.
492 Patterns of microbial abundance and heterotrophic activity along nitrogen and
493 salinity gradients in coastal wetlands. *Aquatic Sciences*, 84, 22,
494 <https://doi.org/10.1007/s00027-022-00855-6>, 2022.

495 Cardona, T., Shao, S., and Nixon, P. J: Enhancing photosynthesis in plants: the light
496 reactions. *Essays in biochemistry*, 62(1), 85-94,
497 <https://doi.org/10.1042/EBC20170015> , 2018.

498 Chen, W., Wolf, B., Zheng, X., Yao, Z., Butterbach-bahl, K. L. A. U. S., Brueggemann,
499 N., ... and Han, X: Annual methane uptake by temperate semiarid steppes as
500 regulated by stocking rates, aboveground plant biomass and topsoil air



- 501 permeability. *Glob. Change Biol.*, 17(9), 2803-2816.
502 <https://doi.org/10.1111/j.1365-2486.2011.02444.x>, 2011.
- 503 Comín, F. A., Julia, R., Comin, M. P., and Plana, F: Hydrogeochemistry of Lake
504 Gallocanta (Aragón, NE Spain). In *Saline Lakes: Proceedings of the Fourth*
505 *International Symposium on Athalassic (inland) Saline Lakes*, held at Banyoles,
506 Spain, May 1988 (pp 51-66). Springer Netherlands, 1990
- 507 Deng, Y., Liu, Y., Dumont, M., and Conrad, R. Salinity affects the composition of the
508 aerobic methanotroph community in alkaline lake sediments from the Tibetan
509 Plateau. *Microb. Ecol.*, 73, 101-110, <https://doi.org/10.1007/s00248-016-0879-5>,
510 2017.
- 511 Duarte, C. M., Prairie, Y. T., Montes, C., Cole, J. J., Striegl, R., Melack, J., and Downing,
512 J. A: CO₂ emissions from saline lakes: A global estimate of a surprisingly large
513 flux. *J. Geophys. Res. G: Biogeosciences*, 113(G4),
514 <https://doi.org/10.1029/2007JG000637>, 2008.
- 515 Eugster, H. P., and Hardie, L. A. (1978). Saline lakes. In *Lakes: chemistry, geology,*
516 *physics* (pp. 237-293). New York, NY: Springer New York.
- 517 Feller, U: Drought stress and carbon assimilation in a warming climate: Reversible and
518 irreversible impacts. *J. Plant Physiol.*, 203, 84-94,
519 <https://doi.org/10.1016/j.jplph.2016.04.002>, 2016.
- 520 García, C. M., García-Ruiz, R., Rendón, M., Niell, F. X., and Lucena, J: Hydrological
521 cycle and interannual variability of the aquatic community in a temporary saline
522 lake (Fuente de Piedra, Southern Spain). *Hydrobiologia*, 345, 131-141,
523 <https://doi.org/10.1023/A:1002983723725>, 1997.
- 524 Garcia, C. M., and Niell, F. X: Burrowing beetles of the genus *Bledius* (Staphylinidae) as
525 agents of bioturbation in the emergent areas and shores of an athalassic inland lake
526 (Fuente de Piedra, southern of Spain). *Hydrobiologia*, 215, 163-173,
527 <https://doi.org/10.1007/BF00014719>, 1991.
- 528 García, C. M., and Niell, F. X: Seasonal change in a saline temporary lake (Fuente de
529 Piedra, southern Spain). *Hydrobiologia*, 267(1), 211-223,
530 <https://doi.org/10.1007/BF00018803>, 1993.
- 531 Guerrero, M. C., and Wit, R. d: Microbial mats in the inland saline lakes of Spain.
532 *Limnetica*, 8, 197-204, 1992.
- 533 Hammer, U. T: *Saline lake ecosystems of the world*. Springer Science and Business
534 Media, 1986.



- 535 Hardie, L. A., Smoot, J. P., and Eugster, H. P: Saline lakes and their deposits: a
536 sedimentological approach. *Modern and ancient lake sediments*, 7-41, 1978.
- 537 Hassani, A., Azapagic, A., D'Odorico, P., Keshmiri, A., and Shokri, N: Desiccation crisis
538 of saline lakes: A new decision-support framework for building resilience to
539 climate change. *Sci. Total Environ.*, 703, 134718,
540 <https://doi.org/10.1016/j.scitotenv.2019.134718> , 2020.
- 541 Heiri, O., Lotter, A. F., and Lemcke, G.: Loss on ignition as a method for estimating
542 organic and carbonate content in sediments: reproducibility and comparability of
543 results. *J. Paleolimnol.*, 25, 101-110, <https://doi.org/10.1023/A:1008119611481> ,
544 2001.
- 545 Khmelenina, V. N., Shchukin, V. N., Reshetnikov, A. S., Mustakhimov, I. I., Suzina, N.
546 E., Eshinimaev, B. T., and Trotsenko, Y. A.: Structural and functional features of
547 methanotrophs from hypersaline and alkaline lakes. *Microbiology*, 79, 472-482,
548 <https://doi.org/10.1134/S0026261710040090>, 2010.
- 549 Kljun, N., Calanca, P., Rotach, M. W., and Schmid, H. P.: A simple parameterisation for
550 flux footprint predictions. *Bound-Lay Meteorol.*, 112(3), 503–523,
551 <https://doi.org/10.1023/B:BOUN.0000030653.71031.96> , 2004.
- 552 Ho, A., Mo, Y., Lee, H. J., Sauheitl, L., Jia, Z., and Horn, M. A. Effect of salt stress on
553 aerobic methane oxidation and associated methanotrophs; a microcosm study of a
554 natural community from a non-saline environment. *Soil Biol. Biochem.*, 125, 210-
555 214, <https://doi.org/10.1016/j.soilbio.2018.07.013> , 2018.
- 556 Li, Y., Zhang, C., Wang, N., Han, Q., Zhang, X., Liu, Y., Xu, L. and Ye, W: Substantial
557 inorganic carbon sink in closed drainage basins globally. *Nature Geosci.*, 10(7),
558 501-506, <https://doi.org/10.1038/ngeo2972> , 2017.
- 559 Li, X. Y., Shi, F. Z., Ma, Y. J., Zhao, S. J., and Wei, J. Q: Significant winter CO₂ uptake
560 by saline lakes on the Qinghai-Tibet Plateau. *Glob. Change Biol.*, 28(6), 2041–
561 2052, <https://doi.org/10.1111/gcb.16054> , 2022.
- 562 Liao, Y., Xiao, Q., Li, Y., Yang, C., Li, J., and Duan, H: Salinity is an important factor in
563 carbon emissions from an inland lake in arid region. *Sci. Total Environ.*, 906,
564 167721, <https://doi.org/10.1016/j.scitotenv.2023.167721> , 2024.
- 565 Martínez-García, A., Peralta-Maraver, I., Rodríguez-Velasco, E., Batanero, G.L., García-
566 Alguacil, M., Picazo, F., Calvo, J., Morales-Baquero, R., Rueda, F.J., Reche, R:
567 Particulate organic carbon sedimentation triggers lagged methane emissions in a



- 568 eutrophic reservoir. *Limnol. Oceanogr. Lett.*, <https://doi.org/10.1002/lo2.10379> ,
569 2024.
- 570 Messenger, M. L., Lehner, B., Grill, G., Nedeva, I., and Schmitt, O: Estimating the volume
571 and age of water stored in global lakes using a geo-statistical approach. *Nature*
572 *comm.*, 7(1), 13603, <https://doi.org/10.1038/ncomms13603>, 2016.
- 573 Moncrieff, J. B., Massheder, J. M., de Bruin, H., Elbers, J., Friborg, T., Heusinkveld, B.,
574 Kabat, P., Scott, S., Soegaard, H., and Verhoef, A.: A system to measure surface
575 fluxes of momentum, sensible heat, water vapour and carbon dioxide. *J. Hydrol.*,
576 188–189, 589–611, [https://doi.org/10.1016/S0022-1694\(96\)03194-0](https://doi.org/10.1016/S0022-1694(96)03194-0) ,1997.
- 577 Moncrieff, J., Clement, R., Finnigan, J., and Meyers, T: Averaging, Detrending, and
578 Filtering of Eddy Covariance Time Series. In *Handbook of Micrometeorology*
579 (pp. 7–31), 2004.
- 580 Murguía-Flores, F., Ganesan, A. L., Arndt, S., and Hornibrook, E. R.: Global uptake of
581 atmospheric methane by soil from 1900 to 2100. *Global Biogeochem. Cycles*,
582 35(7), e2020GB006774, <https://doi.org/10.1029/2020GB006774> , 2021.
- 583 Osudar, R., Klings, K. W., Wagner, D., and Bussmann, I.: Effect of salinity on microbial
584 methane oxidation in freshwater and marine environments. *Aquatic Microb. Ecol.*,
585 80(2), 181-192, <https://doi.org/10.3354/ame01845> , 2017.
- 586 Pastorello, G., Trotta, C., Canfora, E., Chu, H., Christianson, D., Cheah, Y. W., ... & Law,
587 B.: The FLUXNET2015 dataset and the ONEFlux processing pipeline for eddy
588 covariance data. *Sci. Data*, 7, 225, <https://doi.org/10.1038/s41597-020-0534-3>,
589 2020.
- 590 Perez-Quezada, J. F., Urrutia, P., Olivares-Rojas, J., Meijide, A., Sánchez-Cañete, E. P.,
591 and Gaxiola, A.: Long term effects of fire on the soil greenhouse gas balance of
592 an old-growth temperate rainforest. *Sci. Total Environ.*, 755, 142442,
593 <https://doi.org/10.1016/j.scitotenv.2020.142442> , 2021.
- 594 Perkins-Kirkpatrick, S. E., and Lewis, S. C.: Increasing trends in regional heatwaves.
595 *Nature comm.*, 11(1), 3357, <https://doi.org/10.1038/s41467-020-16970-7> , 2020.
- 596 Rafalska, A., Walkiewicz, A., Osborne, B., Klumpp, K., and Bieganowski, A.: Variation
597 in methane uptake by grassland soils in the context of climate change–A review
598 of effects and mechanisms. *Sci. Total Environ.*, 871, 162127,
599 <https://doi.org/10.1016/j.scitotenv.2023.162127> , 2023.



- 600 Raymond, P. A., Hartmann, J., Lauerwald, R., Sobek, S., McDonald, C., Hoover, M., ...
601 and Guth, P.: Global carbon dioxide emissions from inland waters. *Nature*,
602 503(7476), 355-359, <https://doi.org/10.1038/nature12760> , 2013.
- 603 Rodríguez- Rodríguez, M., Benavente, J. and Moral, F.: High density ground-water flow,
604 major-ion chemistry and field experiments in a closed basin: Fuente de Piedra
605 Playa Lake (Spain). *American J. Environ. Sciences*. 1, 164–171, 2006.
- 606 Rysgaard, S., Glud, R. N., Lennert, K., Cooper, M., Halden, N., Leakey, R. J. G., and
607 Barber, D.: Ikaite crystals in melting sea ice—implications for pCO₂ and pH levels
608 in Arctic surface waters. *The Cryosphere*, 6(4), 901–908,
609 <https://doi.org/10.5194/tc-6-901-2012> , 2012.
- 610 Rysgaard, S., Søgaard, D. H., Cooper, M., Pućko, M., Lennert, K., Papakyriakou, T. N.,
611 and Barber, D.: Ikaite crystal distribution in Arctic winter sea ice and implications
612 for CO₂ system dynamics. *The Cryosphere*, 7(2), 707–718,
613 <https://doi.org/10.5194/tc-7-707-2013> , 2013.
- 614 Saccò, M., White, N. E., Harrod, C., Salazar, G., Aguilar, P., Cubillos, C. F., ... and
615 Allentoft, M. E.. Salt to conserve: A review on the ecology and preservation of
616 hypersaline ecosystems. *Biol. Rev.*, 96(6), 2828-2850,
617 <https://doi.org/10.1111/brv.12780> , 2021.
- 618 Sabbatini, S., Mammarella, I., Arriga, N., Fratini, G., Graf, A., Hörtnagl, L., Ibrom, A.,
619 Longdoz, B., Mauder, M., Merbold, L., Metzger, S., Montagnani, L., Pitacco, A.,
620 Rebmann, C., Sedláč, P., Šigut, L., Vitale, D., and Papale, D.: Eddy covariance
621 raw data processing for CO₂ and energy fluxes calculation at ICOS ecosystem
622 stations. *Int. Agrophysics.*, 32(4), 495–515, <https://doi.org/10.1515/intag-2017-0043> , 2018.
- 624 Sharkey, T. D.: Effects of moderate heat stress on photosynthesis: importance of
625 thylakoid reactions, rubisco deactivation, reactive oxygen species, and
626 thermotolerance provided by isoprene. *Plant Cell Environ.* 28(3), 269-277,
627 <https://doi.org/10.1111/j.1365-3040.2005.01324.x> , 2005.
- 628 Smith, T. P., Thomas, T. J., García-Carreras, B., Sal, S., Yvon-Durocher, G., Bell, T., and
629 Pawar, S.: Community-level respiration of prokaryotic microbes may rise with
630 global warming. *Nature comm.*, 10(1), 5124, <https://doi.org/10.1038/s41467-019-13109-1> , 2019.
- 632 Song, K. S., Zang, S. Y., Zhao, Y., Li, L., Du, J., Zhang, N. N., ... and Liu, L.:
633 Spatiotemporal characterization of dissolved carbon for inland waters in semi-



- 634 humid/semi-arid region, China. *Hydrol. Earth Syst. Sci.*, 17(10), 4269-4281,
635 <https://doi.org/10.5194/hess-17-4269-2013> , 2013.
- 636 Soued, C., Bogard, M. J., Finlay, K., Bortolotti, L. E., Leavitt, P. R., Badiou, P., ... and
637 Kowal, P.: Salinity causes widespread restriction of methane emissions from small
638 inland waters. *Nature Comm.*, 15(1), 717, <https://doi.org/10.1038/s41467-024-44715-3> , 2024.
- 640 Stoy, P. C., Mauder, M., Foken, T., Marcolla, B., Boegh, E., Ibrom, A., Arain, M. A.,
641 Arneth, A., Aurela, M., Bernhofer, C., Cescatti, A., Dellwik, E., Duce, P.,
642 Gianelle, D., van Gorsel, E., Kiely, G., Knohl, A., Margolis, H., Mccaughey, H.,
643 ... Varlagin, A.: A data-driven analysis of energy balance closure across
644 FLUXNET research sites: The role of landscape scale heterogeneity. *Agric. For.*
645 *Meteorol.*, 171–172, 137–152, <https://doi.org/10.1016/j.agrformet.2012.11.004> ,
646 2013
- 647 Trenberth, K. E.: Changes in precipitation with climate change. *Clim. Res.* 47(1-2), 123-
648 138, <https://doi.org/10.3354/cr00953> , 2011.
- 649 Tweed, S., Grace, M., Leblanc, M., Cartwright, I., and Smithyman, D.: The individual
650 response of saline lakes to a severe drought. *Sci. Total Environ.*, 409(19), 3919-
651 3933, <https://doi.org/10.1016/j.scitotenv.2011.06.023> ,2011.
- 652 Vickers, D., and Mahrt, L.: Quality control and flux sampling problems for tower and
653 aircraft data. *J. Atmos. Ocean. Techno.*, 14(3), 512–526.,
654 [https://doi.org/10.1175/1520-0426\(1997\)014<0512:QCAFSP>2.0.CO;2](https://doi.org/10.1175/1520-0426(1997)014<0512:QCAFSP>2.0.CO;2) , 1997.
- 655 Wang, J., Song, C., Reager, J. T., Yao, F., Famiglietti, J. S., Sheng, Y., ..., and Wada, Y.:
656 Recent global decline in endorheic basin water storages. *Nature Geosci* 11, 926–
657 932, <https://doi.org/10.1038/s41561-018-0265-7> , 2018.
- 658 Webb, E. K., Pearman, G. I., and Leuning, R. Correction of flux measurements for density
659 effects due to heat and water vapour transfer. *Q. J. R. Meteorol. Soc.* 106 (447),
660 85–100, <https://doi.org/10.1002/qj.49710644707> ,1980
- 661 Wen, Z., Song, K., Shang, Y., Fang, C., Li, L., Lv, L., ... and Chen, L.: Carbon dioxide
662 emissions from lakes and reservoirs of China: a regional estimate based on the
663 calculated pCO₂. *Atmos. Environ.*, 170, 71-81,
664 <https://doi.org/10.1016/j.atmosenv.2017.09.032> , 2017.
- 665 Williams, W. D.: Environmental threats to salt lakes and the likely status of inland saline
666 ecosystems in 2025. *Environ. Conserv.*, 29(2), 154-167,
667 <https://doi.org/10.1017/S0376892902000103> , 2002.



- 668 Wilson, K., Goldstein, A., Falge, E., Aubinet, M., Baldocchi, D., Berbigier, P., ... &
669 Verma, S.: Energy balance closure at FLUXNET sites. *Agricultural and Forest*
670 *Meteorology*, 113(1–4), 223–243, [https://doi.org/10.1016/S0168-1923\(02\)00109-](https://doi.org/10.1016/S0168-1923(02)00109-0)
671 [0](https://doi.org/10.1016/S0168-1923(02)00109-0), 2002.
- 672 Wu, Y., Wang, N., Zhao, L., Zhang, Z., Chen, L. I., Lu, Y., Lü, X., and Chang, J.:
673 Hydrochemical characteristics and recharge sources of Lake Nuertu in the
674 Badain Jaran Desert. *Sci. Bull.*, 59(9), 886–895, [https://doi.org/10.1007/s11434-](https://doi.org/10.1007/s11434-013-0102-8)
675 [013-0102-8](https://doi.org/10.1007/s11434-013-0102-8), 2014.
- 676 Wurtsbaugh, W. A., Miller, C., Null, S. E., DeRose, R. J., Wilcock, P., Hahnenberger,
677 M., ... and Moore, J.: Decline of the world's saline lakes. *Nat. Geosci.*, 10(11),
678 816–821, <https://doi.org/10.1038/ngeo3052>, 2017
- 679 Yan, L., and Zheng, M.: Influence of climate change on saline lakes of the Tibet Plateau,
680 1973–2010. *Geomorphology*, 246, 68–78,
681 <https://doi.org/10.1016/j.geomorph.2015.06.006>, 2015.
- 682 Yang, P., Wang, N. A., Zhao, L., Zhang, D., Zhao, H., Niu, Z., and Fan, G.: Variation
683 characteristics and influencing mechanism of CO₂ flux from lakes in the Badain
684 Jaran Desert: A case study of Yindeer Lake. *Ecol. Ind.*, 127, 107731,
685 <https://doi.org/10.1016/j.ecolind.2021.107731>, 2021.
- 686 Yvon-Durocher, G., Caffrey, J. M., Cescatti, A., Dossena, M., Giorgio, P. D., Gasol, J.
687 M., ... and Allen, A. P.: Reconciling the temperature dependence of respiration
688 across timescales and ecosystem types. *Nature*, 487(7408), 472–476,
689 <https://doi.org/10.1038/nature11205>, 2012.
- 690 Yvon-Durocher, G., Jones, J. I., Trimmer, M., Woodward, G. and Montoya, J. M.:
691 Warming alters the metabolic balance of ecosystems. *Phil. Trans. R. Soc. B* 365,
692 2117–2126, <https://doi.org/10.1098/rstb.2010.0038>, 2010.



FIGURES

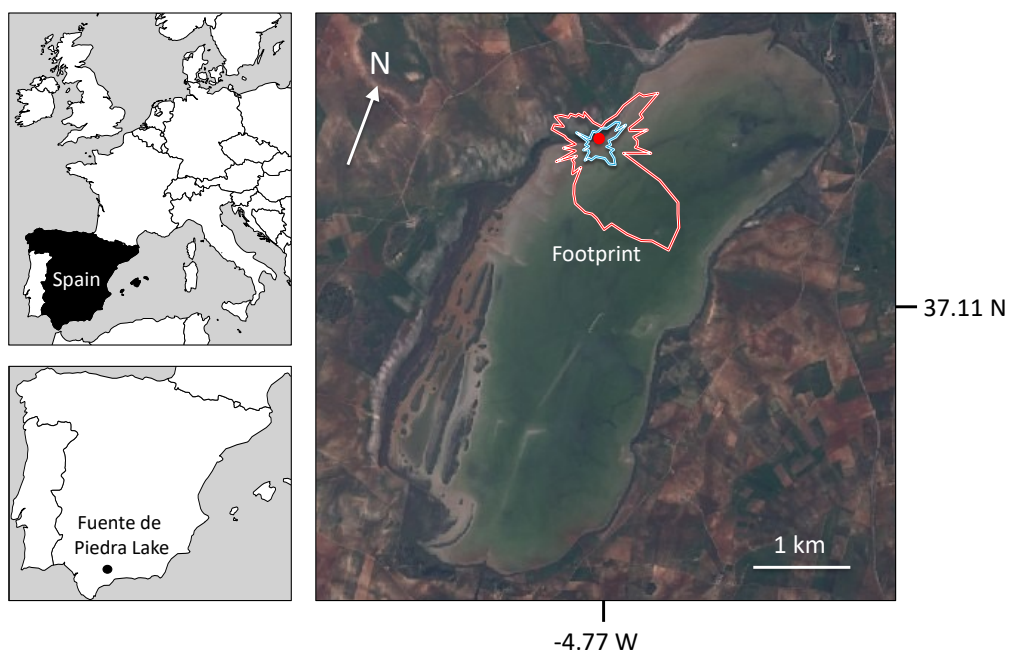


Fig 1. Location of the Fuente de Piedra Lake (province of Málaga, South of Spain). Dot inside polygon in right panel shows the location of the eddy covariance tower. The areas within the footprint contributing the 90% to measured fluxes are delimited inside polygons for daytime (blue) and nighttime (red).

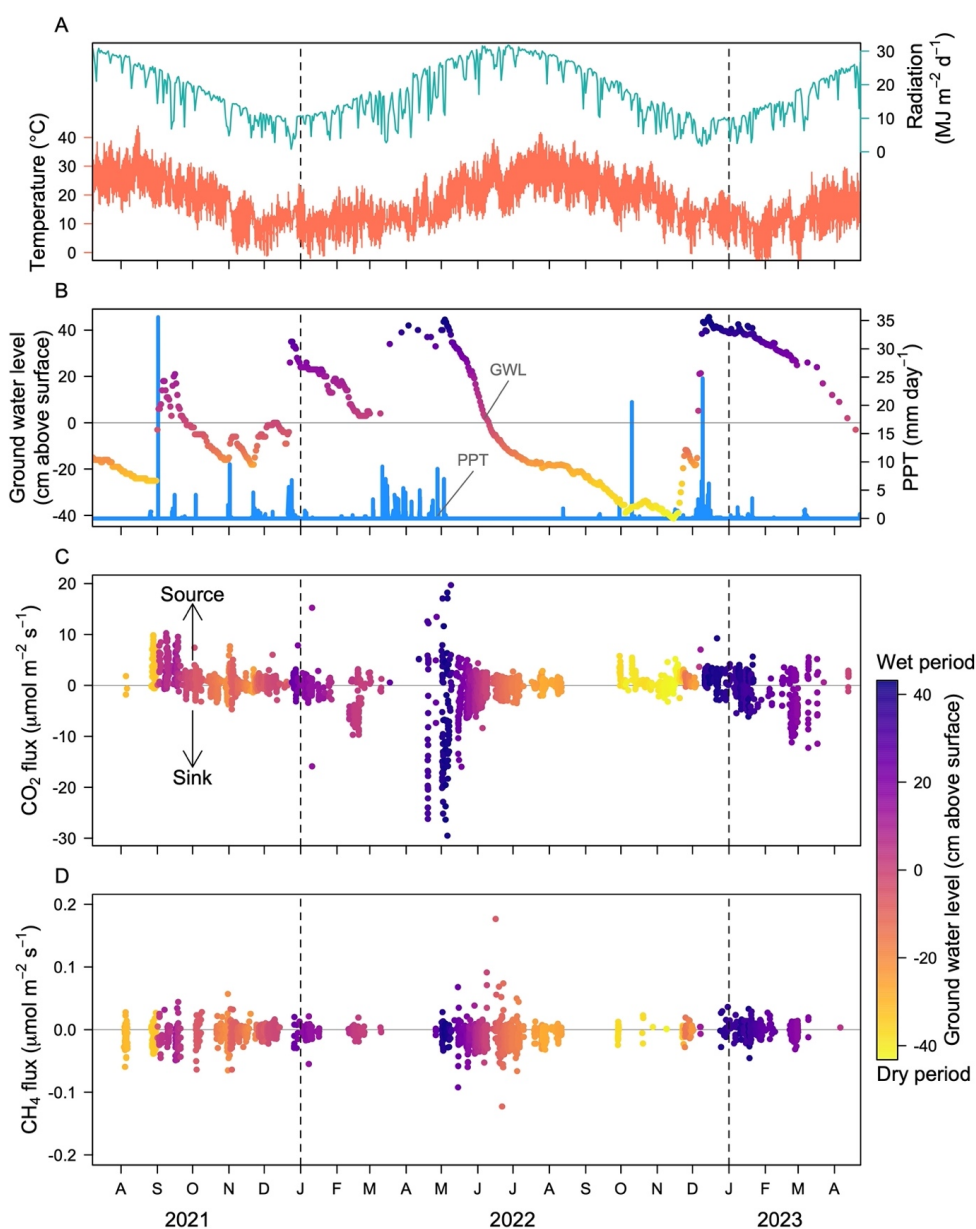


Fig 2. Time series of (A) air temperature and incident solar radiation, (B) groundwater level and precipitation (PPT), (C) CO₂ and (D) CH₄ flux, collected at Fuente de Piedra Lake during 2021, 2022, and 2023.

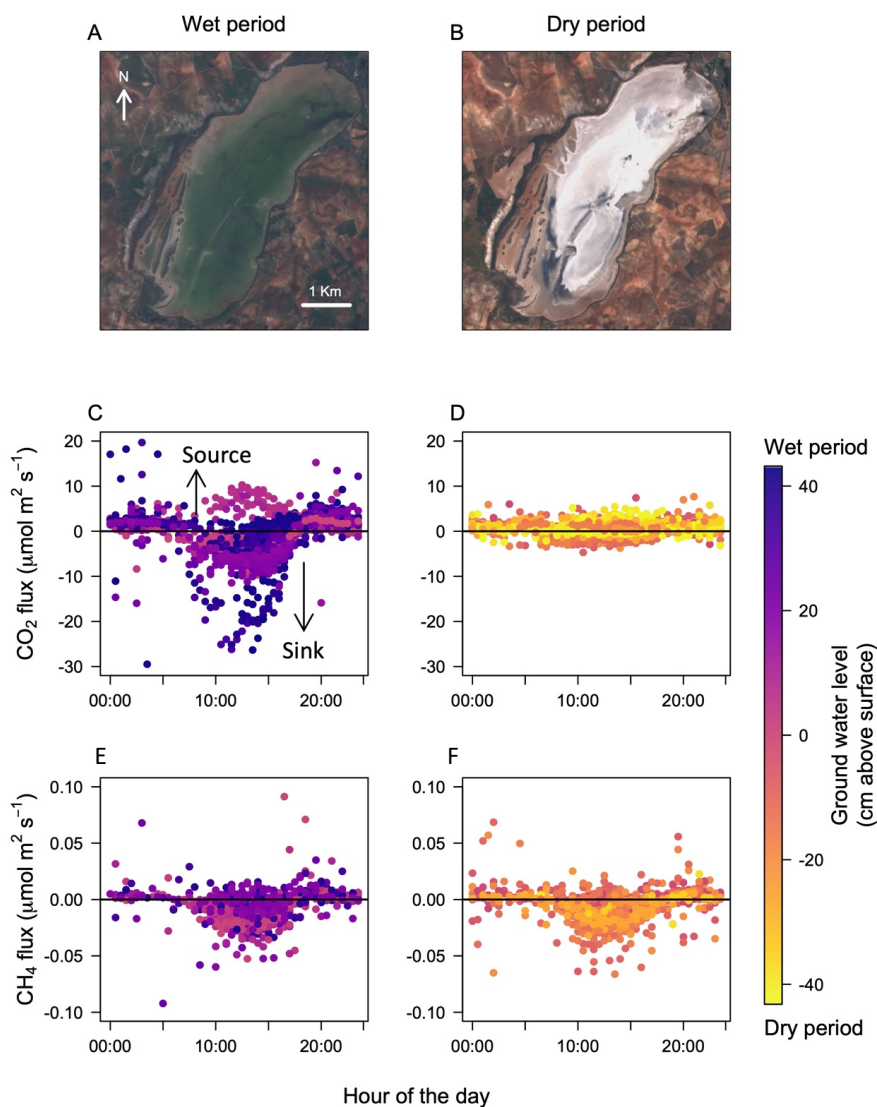


Fig 3. Aerial photos of Fuente de Piedra Lake during a period of maximum water availability (wet period, **A**) and during a typical dry episode (**B**). Note that for some period during the dry episodes, a salt crust forms covering practically the entire extent of the lake. The figure shows the daily pattern of CO₂ and CH₄ fluxes during the wet period (**C** and **E** respectively) and the dry period (**D** and **F** respectively). Water availability is measured in terms of ground water level.

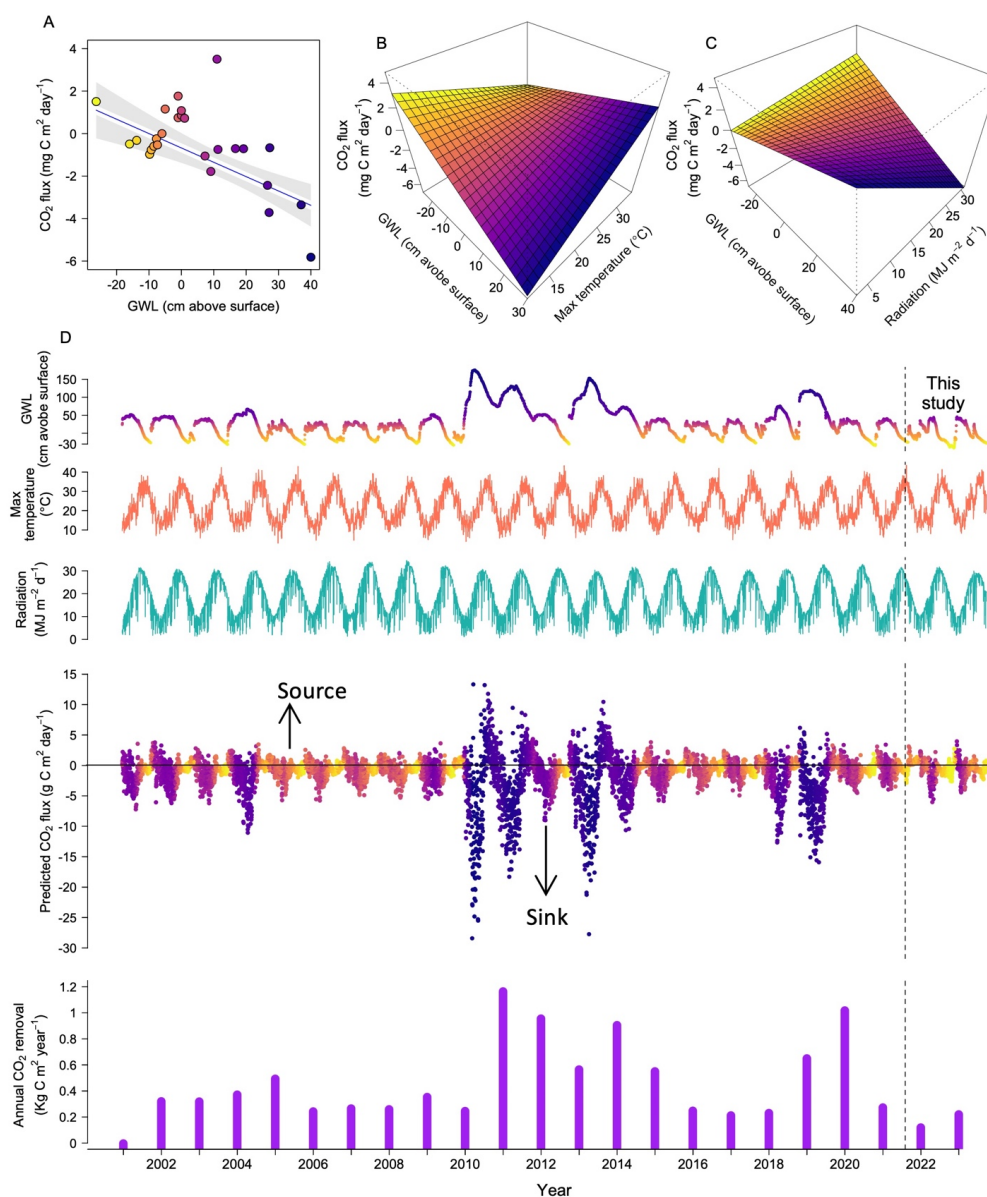


Fig 4. Prediction of CO₂ flux as a response to groundwater level (A), the interaction between groundwater level and daily maximum temperature (B), and the interaction between groundwater level and incident solar radiation (C). Using existing time series for the model predictors, it has been possible to reconstruct the estimated CO₂ fluxes, as well as the annual cumulative value of CO₂ removal since 2001 for Fuente de Piedra Lake (D).